Makara J. Technol. 22/3 (2018), 123-128
doi: 10.7454/mst.v22i3.3645

Transition Metal Dichalcogenide for High-Performance Electrode of Supercapacitor

Saifful Kamaluddin Muzakir[1*], Ahmad Salihin Samsudin[1], and Bouchta Sahraoui[2]

1. Material Technology Programme, Faculty of Industrial Sciences & Technology, Universiti Malaysia Pahang, Lebuhraya Tun Razak, Gambang 26300, Malaysia
2. Laboratory POMA, UMR CNR 6136, University of Angers, 2 Boulevard Lavoisier, 49045 Angers, France

[*]*e-mail: saifful@ump.edu.my*

Abstract

Molybdenum dichalcogenides have been reviewed from the perspectives of bandgap, conductivity, and oxidation states of transition metal. Researchers have concluded that a narrow-bandgap transition metal dichalcogenide with high conductivity could be achieved for the high-performance electrode of a supercapacitor.

Abstrak

Logam Transisi Dikalkogenida untuk Elektroda Superkapasitor Kinerja Tinggi. Molibdenum dikalkogenida telah dikaji ulang dari perspektif keadaan-keadaan celah pita, konduktivitas, dan oksidasi logam transisi; yang menyimpulkan bahwa suatu logam transisi dikalkogenida celah pita sempit dengan konduktivitas tinggi dapat digunakan untuk elektroda superkapasitor kinerja tinggi.

Keywords: supercapacitor, transition metal dichalcogenide

1. Introduction

Supercapacitors (SCs) are energy storage devices that could store and release large amounts of charges in a short period (approximately from 1 s to 30 s), which result in high energy and power density properties, respectively. The properties of SCs are in between those of capacitors (low energy and high power densities) and batteries (high energy and low power densities). The development of SCs with enhanced charge storage properties and fast charge and discharge timescales would expedite the deployment of SCs in various domains. Archetypical symmetric SCs are fabricated using two activated carbon (AC) electrodes (working potential, approximately from 0 V to −0.9 V) [1] separated by aqueous electrolyte. The potential window could be widened by replacing the AC electrode with pseudo-capacitor (PC)-type material, which exhibits different potential windows in different regions of voltage (e.g., from 0 V to 0.7 V for Mo_9Se_{11}) [2]. Typical devices could be regarded as asymmetric or hybrid SCs, which employ two charge storage mechanisms, viz., (i) electrostatic-based process at the electrolyte–AC electrode interface and (ii) faradaic-based process at the surface and bulk of the PC electrode [3]. Stemming from the dire need to increase the energy density without compromising the power density, a fundamental approach of material selection for the PC electrode is needed to identify characteristics that satisfy the requirements. Transition metal dichalcogenides (TMDs), e.g., MoS_2 and $MoSe_2$, are widely used as PC electrode because of their layered structure, which could be utilized as a medium for reversible charge storage. TMD-based electrodes exhibited promising progress in recent years. Thus, TMD-based electrodes are considered good candidates for PC electrode. Layered-structure TMDs have been the focus of numerous research activities because of the similarity of their structure to that of graphene. Furthermore, the development of graphene-based electronics is restricted because of the drastic electron mobility drop, i.e., from approximately 2×10^5 $cm^2/(V \cdot s)$ to 200 $cm^2/(V \cdot s)$, during the opening of a nonzero bandgap [4],[5]. The presence of bandgaps in TMDs consequently broadens their applications in optoelectronics. An indirect bandgap bulk TMD (e.g., 1.33 eV in $MoSe_2$) [6] exhibits a low electron mobility of approximately 160 $cm^2/(V \cdot s)$ [7]. Multilayered TMDs are stacked and bonded by weak Van der Waals forces; therefore, an ultrathin layer of TMD could be peeled off mechanically. The strong covalently bonded transition metal and chalcogenide

atoms in each layer would sustain the mechanical exfoliation process; therefore, the layered structure could be maintained [8]. Manipulation of the ultrathin layer of TMD induces bandgap transition from an indirect (bulk TMD) bandgap to a direct (thin layer) bandgap [9]–[11]. A similar transition is observed in germanium, which resulted in a very high electron mobility of single-layer Ge, i.e., approximately 18,195 $cm^2/(V \cdot s)$ (fivefold increment from bulk Ge) [12]. The high electron mobility could be due to the suppression of electron–phonon scattering [13],[14]. Therefore, in principle, TMDs would replace graphene.

2. Methods

In this study, our target is to determine the fundamental properties of molybdenum dichalcogenides, MoX_2 (where X = O, S, Se, Te, and Po), which could provide beneficial insights into the improvement of the performances of SCs. We have identified that the molecular weight (MW), conductivity, band structures of molybdenum dichalcogenides, and oxidation states of molybdenum play important roles in the stated interest. Recent advancement of molybdenum disulfide-based electrodes and its comparison with that of other metal chalcogenide-based electrodes are also included. Researchers have exerted experimental efforts, focusing on some perspectives, viz., (i) synthesis techniques that successfully materialized various TMDs, e.g., Hg_7Se_{10}, [15] tungsten chalcogenides, [16] hollow sphere copper chalcogenides, [17] epitaxially grown cadmium chalcogenides, [18] seed-mediated CdSe, [19] ternary TMDs, [20] and molecularly controlled synthesis of cadmium chalcogenides [21]. (ii) Fundamental studies of new types of TMDs, such as silver chalcogenides, [22] lanthanum-doped TMDs, [23] rhenium chalcogenides, [24] and vanadium chalcogenides, [25] were also conducted to obtain insights into prospective applications. (iii) The fabrication of TMD-based devices for various applications was achievable because of concentrated work in earlier activities, e.g., piezoelectric devices, [26] biological and industrial applications, [27] photonic devices, [28] electrochemical devices, [29] gas sensor, [30] energy storage, [31],[32] and electrocatalyst [33].

The theoretical approach was also employed to analyze fascinating material properties, which are not experimentally feasible. Cundari *et al.* successfully simulated realistic clusters of several TMDs using the GAMESS program package, which could lead to the unlimited exploration of realistic virtual experiments employing TMDs [34]. Gautier *et al.* examined the electronic structures (i.e., bandgaps, band structures, and electronic densities) of some electron-rich TMDs using density functional theory (DFT) calculations [35]. The calculations were conducted using local density approximation, Becke exchange and Perdew correlation, nonlocal gradient correction functionality, and uncontracted triple-ξ Slater-type orbital basis set. High-accuracy calculation of the electronic properties of TMDs were obtained by Li *et al.* with modest computational costs at the HSE06 and TB-mBJ levels of DFT [36]. In the following year, Lin *et al.* utilized a combination of theoretical calculations and experimental work to analyze the structural flexibility of TMDs [37]. Their work proved that the structure of TMDs could be tailored because of their capability to accommodate large torsional twist, resulting in tunable electronic properties.

3. Results and Discussion

The pseudocapacitive properties of TMDs are rooted from the contributions of two major charge storage mechanisms, viz., redox pseudocapacitance (Fig. 1a) and intercalation pseudocapacitance (Fig. 1b) [38]. Redox pseudocapacitance involves the chemisorption of electrolyte cations (e.g., Li^+) on the surface of TMD (e.g., $MoSe_2$ with Mo oxidation states of +4, +5, and +6), [39] with simultaneous faradaic charge transfer. Intercalation pseudocapacitance occurs due to the intercalation of the electrolyte cations into bulk layers of TMD. The cations are subsequently chemisorbed on the surface of TMD, with simultaneous faradaic charge transfer.

Mo^{+6} could be reduced to Mo^{+5} or Mo^{+4}, corresponding to electron transfer during the charging process. The electron is subsequently transferred to the cations; Li^+ ions are reduced and chemisorbed on the surface of TMD. The mechanism is reversible. The speed of electron transfer is correlated to that of the speed of the charge storage (charging) and removal (discharging) processes. Electrons travel in the bulk TMD at drift velocity, υ_d, which is obtained using the equation:

$$\upsilon_d = \mu \times E \tag{1}$$

where μ is the electron mobility and E is the applied electric field. The electron mobility is related to the conductivity of the TMD, which is represented by the equation:

$$\sigma = \eta \times e \times \mu \tag{2}$$

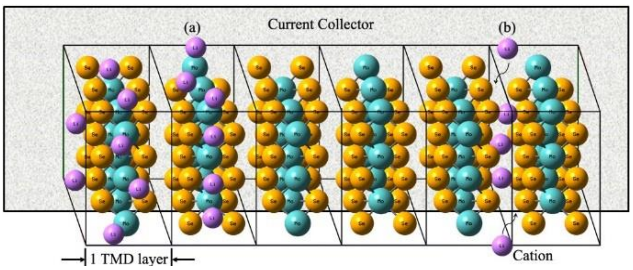

Figure 1. Representation of (a) redox pseudocapacitance and (b) intercalation pseudocapacitance charge storage mechanism at the surface and bulk of TMD, respectively.

where σ is the conductivity, η is the concentration of the electron, and e is the charge of the electron [4]. The electron mobility is correlated with the effective mass of the electron, m_e^*, as expressed using the following equation:

$$\mu = (e \times \tau) / m_e^* \quad (3)$$

where τ is the time of relaxation between two electron scattering incidents in the TMD, which originated from defects or impurities, i.e., lattice vibrations and phonons [4,5]. The electric field is applied during charging of the SC; therefore, its presence is considered in the energy band theory, which was established on the basis of the effective mass theorem [40–42]. Wang *et al.* [5] successfully derived the effective mass–bandgap relation using DFT and a tight-binding model of graphene, establishing the following linear correlation:

$$m_e^* = \left(2\hbar^2 / 9t_o^2 r_o^2\right) E_G \quad (4)$$

where $\hbar$ is the reduced Plank's constant, r_o is the equilibrium bond length, t_o is the electron hopping parameter, [43] and E_G is the bandgap. Therefore, narrow-bandgap TMDs would have low effective mass of electrons, which will lead to high electron mobility and conductivity. A narrow-bandgap TMD-based electrode could exhibit higher power density than wide-bandgap TMDs because of higher speed of charge transfer.

Narrow-bandgap (approximately 1.54 eV) [44] MoS_2-based electrode exhibited a specific capacitance, C_s, of 376 F/g using 1 M Na_2SO_4 electrolyte (Fig. 2) [45]. Carbon–MoS_2 composites were used to increase the conductivity of the electrode, yielding a higher C_s than that of bare MoS_2-based electrode of approximately 453 F/g using multiwall carbon nanotube–MoS_2 electrode and 1 M Na_2SO_4 electrolyte [46]. C_s is further enhanced with the incorporation of conducting polymers, which exhibited a C_s value of 575 F/g when using polyaniline–MoS_2 electrode and 1 M H_2SO_4 electrolyte system [47]. Other TMD–electrodes, i.e., CoS (1,314 F/g), [48] Ni_3S_2/MoS_2 (848 F/g), [49] WS_2/carbon tube (350 F/g), [50] and WSe_2 (2 F/g), [51] have been investigated. However, these electrodes were fabricated using various types of optimization, e.g., type and concentration of electrolyte, morphology of material, and technique of synthesis, which would lead to different degrees of contribution to the cumulative C_s.

One-dimensional nanostructures (e.g., nanorods and nanoneedles) could be grown on the layered structure of TMDs. The nanostructures could accommodate and facilitate fast redox reactions, consequently increasing the power density. However, extended size reduction of one-dimensional structures in the strong quantum confinement region (size of TMD < exciton Bohr radius) would increase the bandgap of the TMD because of the quantum confinement effect [65]. Increment of the bandgap sacrifices electron mobility and conductivity, leading to a low power density. This observation opens up the opportunity for structure manipulation of narrow-bandgap TMDs with small exciton Bohr radius as PC electrode. A typical example is $MoSe_2$, which has a small exciton Bohr radius of approximately 2.40 nm, [66] narrow bandgap of 1.33 eV, [6] and effective mass of electron 4.46×10^{-31} kg [66]. Size reduction of the weak quantum confinement region (>2.40 nm) would not jeopardize the electron mobility and conductivity.

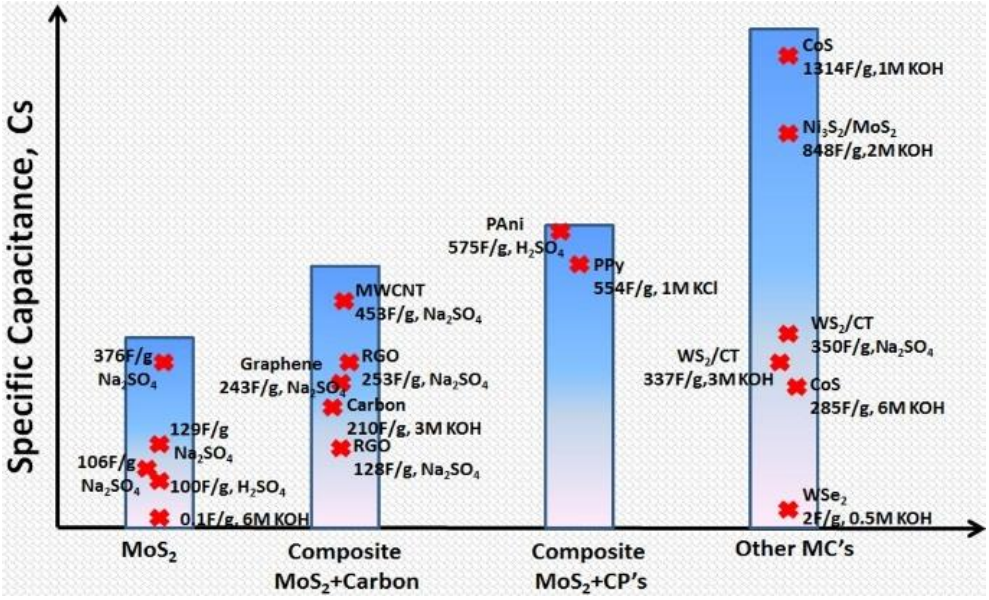

Figure 2. Specific capacitance, C_s, obtained by TMDs-based electrode with various types of optimization [45–64].

A TMD-based electrode with high energy density (approximately 42 Wh/kg), power density (approximately 960 W/kg), and specific capacitance C_s (approximately 510 F/g) is achieved using hierarchical Mo_9Se_{11} nanoneedles (cross-sectional diameter of 10–20 nm) electrode in our recent work [2]. The excellent electrochemical properties could be attributed to the high electron conductivity. Bulk Mo dichalcogenides exhibited indirect bandgaps (Table 1), indicating a high effective mass of electron [67] that leads to low electron mobility and conductivity. Manipulation of thin-layer TMD using strain engineering, [68] thermal decoupling, [67] and mechanical exfoliation [69] techniques have been reported to induce a transition from indirect bandgap to direct bandgap. The reported bandgaps in Table 1 are divided into two categories, i.e., indirect bandgap (I) and direct bandgap (D), which correspond to bulk and thin-layer TMDs, respectively. The trend of the bandgap with respect to the MW of TMDs predicted that $MoPo_2$ would have the smallest bandgap (approximately 0.33 and 0.29 eV for the indirect and direct bandgaps, respectively) among the other Mo-based dichalcogenides (Fig. 3). Therefore, high electron mobility and conductivity are expected.

The conductivity of thin-layer TMDs is yet to be reported; however, the conductivity of bulk $MoPo_2$ is predicted to be approximately 40.20 S/m. An electrode employing thin-layer $MoPo_2$ has never been demonstrated to date.

The plasma-assisted nanofabrication technique could fabricate two-dimensional metal chalcogenide layers (including $MoPo_2$), as recently claimed by the Colorado School of Mines [80]. The technique could be explored for fabrication. The indirect and direct bandgaps decreased with the increment of the MW of TMDs, along with increment of conductivity. Bulk MoO_2 presented extremely high conductivity (approximately 10,000 S/m) [70,71] despite its wide bandgap. The metal-like conductivity could be attributed to three reasons, i.e., (i) existence of delocalized electron in the valence band, [72] (ii) low contamination of insulator-type MoO_3, [72] and (ii) highly ordered structure [70]. The conductivity of MoO_2 nanorods is lower than that of the bulk (approximately 190 S/m) [72]. MoO_2-based electrodes have exhibited promising energy storage properties, [71,81] but are yet to be deployed in the industrial domain. Transition metals in TMDs play a significant role in the electron transfer process. Transition metals could have multiple oxidation states because of their valence electron configuration in *d*-orbitals, which could be occupied by 10 electrons. Molybdenum with an electron configuration of [Kr] $5s^1$ $4d^5$ indicates that the highest possible oxidation state is +6, corresponding to number of unpaired electrons in the 5*s* and 4*d* orbitals. Other oxidation states of Mo that could exist are +4 and +5. The unpaired electrons are unstable and could take part in chemical bonds with chalcogenides and cations in electrolyte.

Table 1. Properties of Bulk and Thin-layer (TL) MoO_2, MoS_2, $MoSe_2$, $MoTe_2$, and $MoPo_2$

TMDs	MW (g/mol)	σ (S/m)	E_g (eV)	Ox. States
$MoO_{2\ Bulk}$	127.95	10,000 [70,71]	2.42(I) [73]	+4, +5, +6
$MoO_{2\ TL}$		190 [72]	3.85(D) [74]	[75]
$MoS_{2\ Bulk}$	160.07	0.3 [44]	1.54(I) [67]	+4, +5, +6
$MoS_{2\ TL}$		NIL	1.89(D) [67]	[75]
$MoSe_{2\ Bulk}$	253.89	10.0 [44]	1.33(I) [6]	+4, +5, +6
$MoSe_{2\ TL}$		NIL	1.55(D) [67]	[76,77]
$MoTe_{2\ Bulk}$	351.15	22.0 [78]	0.88(I) [69]	+4, +5, +6
$MoTe_{2\ TL}$		NIL	1.02(D) [69]	[79]
$MoPo_{2\ Bulk}$	513.95	40.2	0.33(I)	NIL
$MoPo_{2\ TL}$		NIL	0.29(D)	

[a]Ox. States = oxidation states of Mo

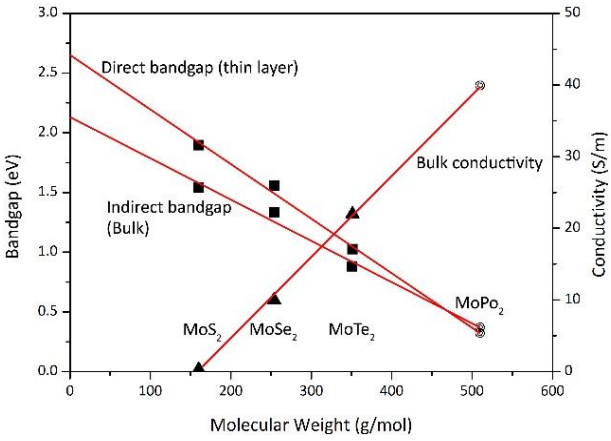

Figure 3. Prediction of direct (approximately 0.29 eV) and indirect (approximately 0.33 eV) bandgaps and conductivity of bulk (approximately 40.20 S/m) $MoPo_2$, marked by hollow circles.

Multiple simultaneous processes are speculated during charging, viz., (i) reversible reduction of Mo^{+6} to Mo^{+5} or Mo^{+4}, which stores charges in Mo temporarily, (ii) electron transfer from TMD (e.g., $MoSe_2$) to cations, and (iii) reversible reduction of cations, which also stores charges temporarily. The accumulation of electrons and charges (cations) would increase the cumulative C_s. Electrolytes containing multiple oxidation state metals have been investigated intensively to yield a high-capacity battery [82,83]. A similar concept could be adopted in the screening of transition metals for PC electrode with high C_s. Manganese with an electron configuration of [Ar] $4s^2$ $3d^5$ exhibits the highest oxidation state, i.e., +7 among the first row of transition metals (i.e., Sc, Ti, V, Cr, Fe, Co, Ni, Cu, and Zn). Other oxidation states of Mn are +2, +3, +4, +5, and +6. Electrodes employing MnO_2 theoretically yielded high C_s of 1,233 F/g, [38] but yielded a C_s of 200 F/g in experiments because of the low conductivity of MnO_2 (approximately 0.00005 S/m) [84].

4. Conclusion

In conclusion, seven parameters affect the specific capacitance (C_s), energy density, and power density of a TMD-based PC electrode, viz., (i) bandgap, (ii) electron effective mass, (iii) electron mobility, (iv) electron conductivity, (v) electron drift velocity, (vi) MW, and (vii) oxidation potential of transition metal. A transition metal with multiple oxidation states is targeted for the synthesis of narrow-bandgap TMDs, which could exhibit high C_s and electron conductivity. The narrow bandgap and high conductivity of thin-layer $MoPo_2$ are predicted. However, a feasible fabrication technique of the thin layer needs to be established.

Acknowledgement

This work is funded by the Research & Innovation Department of University Malaysia Pahang and the Ministry of Education of Malaysia through the Fundamental Research Grant Scheme (RDU 150111).

References

[1] W. Zhang, H. Lin, H. Lu, D. Liu, J. Yin, Z. Lin, J. Mater. Chem. A. 3 (2015) 4399-4404.
[2] R.A. Aziz, S.K. Muzakir, I.I. Misnon, J. Ismail, R. Jose, J. Alloy. Compd. 673 (2016) 390-398.
[3] S. Zhang, N. Pan, Adv. Energy Mater. 5 (2015)
[4] K.I. Bolotin, K.J. Sikes, Z. Jiang, M. Klima, G. Fudenberg, J. Hone, P. Kim, H.L. Stormer, Solid. State Commun. 146 (2008) 351-355.
[5] J. Wang, R. Zhao, M. Yang, Z. Liu, Z. Liu, J. Chem. Phys. 138 (2013) 084701.
[6] Y. Cheng, U. Schwingenschlögl, MoS2: Materials, Physics and Devices, 1 ed., Springer International Publishing, Switzerland, 2014, p.291
[7] B. Chamlagain, Q. Li, N.J. Ghimire, H.-J. Chuang, M.M. Perera, H. Tu, Y. Xu, M. Pan, D. Xaio, J. Yan, D. Mandrus, Z. Zhou, ACS Nano. 8 (2014) 5079-5088.
[8] J. Li, N.V. Medhekar, V.B. Shenoy, J. Phys. Chem. C. 117 (2013) 15842-15848.
[9] M. Hosseini, M. Elahi, M. Pourfath, D. Esseni, Appl. Phys. Lett. 107 (2015) 253503.
[10] J.C. Shaw, H. Zhou, Y. Chen, N.O. Weiss, Y. Liu, Y. Huang, X. Duan, Nano Res. 7 (2015) 511-517.
[11] Y. Zhang, T.-R. Chang, B. Zhou, Y.-T. Cui, H. Yan, Z. Liu, F. Schmitt, J. Lee, R. Moore, Y. Chen, H. Lin, H.-T. Jeng, S.-K. Mo, Z. Hussain, A. Bansil, Z.-X. Shen, Nat. Nano. 9 (2014) 111-115.
[12] E. Bianco, S. Butler, S. Jiang, O.D. Restrepo, W. Windl, J.E. Goldberger, ACS Nano. 7 (2013) 4414-4421.
[13] O.D. Restrepo, R. Mishra, J.E. Goldberger, W. Windl, J. Appl. Phys. 115 (2014) 033711.
[14] L.E. Smart, E.A. Moore, Solid State Chemistry: An Introduction, 3 ed., CRC Press Taylor & Francis Group, Singapore, 2005.
[15] K.W. Kim, M.G. Kanatzidis, Inorg. Chem. 30 (1991) 1966-1969.
[16] R.W.M. Wardle, S. Bhaduri, C.N. Chau, J.A. Ibers, Inorg. Chem. 27 (1988) 1747-1755.
[17] M. Pang, H.C. Zeng, Langmuir. 26 (2010) 5963-5970.
[18] M.I.B. Utama, Z. Peng, R. Chen, B. Peng, X. Xu, Y. Dong, L.M. Wong, S. Wang, H. Sun, Q. Xiong, Nano Lett. 11 (2011) 3051-3057.
[19] R. Xie, M. Zhou, Chem. Mater. 27 (2015) 3055-3064.
[20] A. Eichhöfer, O. Hampe, S. Lebedkin, F. Weigend, Inorg. Chem. 49 (2010) 7331-7339.
[21] T.P.A. Ruberu, H.R. Albright, B. Callis, B. Ward, J. Cisneros, H.-J. Fan, J. Vela, ACS Nano. 6 (2012) 5348-5359.
[22] A. Sahu, L. Qi, M.S. Kang, D. Deng, D.J. Norris, J. Am. Chem. Soc. 133 (2011) 6509-6512.
[23] A. Kornienko, L. Huebner, D. Freedman, T.J. Emge, J.G. Brennan, Inorg. Chem. 42 (2003) 8476-8480.
[24] T.G. Gray, C.M. Rudzinski, E.E. Meyer, R.H. Holm, D.G. Nocera, J. Am. Chem. Soc. 125 (2003) 4755-4770.
[25] C. Simonnet-Jégat, F. Sécheresse, Chem. Rev. 101 (2001) 2601-2612.
[26] M.M. Alyörük, Y. Aierken, D. Çakır, F.M. Peeters, C. Sevik, J. Phys. Chem. C. 119 (2015) 23231-23237.
[27] E.I. Stiefel, Transition Metal Sulfur Chemistry: Biological and Industrial Significance and Key Trends, Transition Metal Sulfur Chemistry, American Chemical Society, 1996, pp.2-38.
[28] M.V. Kovalenko, R.D. Schaller, D. Jarzab, M.A. Loi, D.V. Talapin, J. Am. Chem. Soc. 134 (2012) 2457-2460.
[29] X. Chia, A.Y.S. Eng, A. Ambrosi, S.M. Tan, M. Pumera, Chem. Rev. 115 (2015) 11941-11966.
[30] D. Sarkar, X. Xie, J. Kang, H. Zhang, W. Liu, J. Navarrete, M. Moskovits, K. Banerjee, Nano Lett. 15 (2015) 2852-2862.
[31] P.S.E. Yeo, M.-F. Ng, Chem. Mater. 27 (2015) 5878-5885.
[32] D. Chen, G. Ji, B. Ding, Y. Ma, B. Qu, W. Chen, J.Y. Lee, Ind. Eng. Chem. Res. 53 (2014) 17901-17908.
[33] R.D. Nikam, A.-Y. Lu, P.A. Sonawane, U.R. Kumar, K. Yadav, L.-J. Li, Y.-T. Chen, ACS Appl. Mater. Interfaces. 7 (2015) 23328-23335.
[34] T.R. Cundari, P.D. Raby, J. Phys. Chem. A. 101 (1997) 5783-5788.
[35] R. Gautier, E. Furet, J.-F. Halet, Z. Lin, J.-Y. Saillard, Z. Xu, Inorg. Chem. 41 (2002) 796-804.
[36] W. Li, C.F.J. Walther, A. Kuc, T. Heine, J. Chem. Theory Comput. 9 (2013) 2950-2958.
[37] J. Lin, Y. Zhang, W. Zhou, S.T. Pantelides, ACS Nano. 10 (2016) 2782-2790.

[38] V. Augustyn, P. Simon, B. Dunn, Energy Environ. Sci. 7 (2014) 1597-1614.
[39] J.G. Stark, J. Chem. Educ. 46 (1969) 505.
[40] J.M. Luttinger, W. Kohn, Phys. Rev. 97 (1955) 869-883.
[41] J.C. Slater, Phys. Rev. 76 (1949) 1592-1601.
[42] G.H. Wannier, Phys. Rev. 52 (1937) 191-197.
[43] J. Singleton, Band Theory and Electronic Properties of Solids, Oxford University Press Inc., New York, 2008.
[44] K.-K. Kam, Physics, Iowa State University, Iowa, 1982.
[45] A. Ramadoss, T. Kim, G.-S. Kim, S.J. Kim, New J. Chem. 38 (2014) 2379-2385.
[46] K.-J. Huang, L. Wang, J.-Z. Zhang, L.-L. Wang, Y.-P. Mo, Energy. 67 (2014) 234-240.
[47] K.-J. Huang, L. Wang, Y.-J. Liu, H.-B. Wang, Y.-M. Liu, L.-L. Wang, Electrochim. Acta. 109 (2013) 587-594.
[48] K.-J. Huang, J.-Z. Zhang, G.-W. Shi, Y.-M. Liu, Mater. Lett. 131 (2014) 45-48.
[49] J. Wang, D. Chao, J. Liu, L. Li, L. Lai, J. Lin, Z. Shen, Nano Energy. 7 (2014) 151-160.
[50] S. Ratha, C.S. Rout, ACS Appl. Mater. Interfaces. 5 (2013) 11427-11433.
[51] D. Chakravarty, D.J. Late, RSC Adv. 5 (2015) 21700-21709.
[52] K.-J. Huang, L. Wang, Y.-J. Liu, Y.-M. Liu, H.-B. Wang, T. Gan, L.-L. Wang, Int. J. Hydrog. Energy. 38 (2013) 14027-14034.
[53] G. Ma, H. Peng, J. Mu, H. Huang, X. Zhou, Z. Lei, J. Power Sources. 229 (2013) 72-78.
[54] H. Wan, X. Ji, J. Jiang, J. Yu, L. Miao, L. Zhang, S. Bie, H. Chen, Y. Ruan, J. Power Sources. 243 (2013) 396-402.
[55] B. Hu, X. Qin, A.M. Asiri, K.A. Alamry, A.O. Al-Youbi, X. Sun, Electrochem. Commun. 28 (2013) 75-78.
[56] K. Krishnamoorthy, G.K. Veerasubramani, S. Radhakrishnan, S.J. Kim, Mater. Res. Bull. 50 (2014) 499-502.
[57] B. Hu, X. Qin, A.M. Asiri, K.A. Alamry, A.O. Al-Youbi, X. Sun, Electrochim. Acta. 100 (2013) 24-28.
[58] K.J. Huang, J.Z. Zhang, G.W. Shi, Y.M. Liu, Electrochim. Acta. 132 (2014) 397-403.
[59] M. Mandal, D. Ghosh, S.S. Kalra, C.K. Das, Int. J. Latest Res. Sci. Technol. 3 (2014) 65-69.
[60] G. Sun, J. Liu, X. Zhang, X. Wang, H. Li, Y. Yu, W. Huang, H. Zhang, P. Chen, Angew. Chem. Int. Edit. 53 (2014) 12576-12580.
[61] X. Han, X. Jiang, S. Yin, Advan. Mater. Res. 773 (2013) 524-529.
[62] E.G. da Silveira Firmiano, A.C. Rabelo, C.J. Dalmaschio, A.N. Pinheiro, E.C. Pereira, W.H. Schreiner, E.R. Leite, Advan. Energy Mater. 4 (2014).
[63] J.M. Soon, K.P. Loh, Electrochem. Solid-State Lett. 10 (2007) A250-A254.
[64] Y. Yang, H. Fei, G. Ruan, C. Xiang, J.M. Tour, Advan. Mater. 26 (2014) 8163-8168.
[65] L.E. Brus, J. Chem. Phys. 80 (1984) 4403-4409.
[66] G. Wang, I.C. Gerber, L. Bouet, D. Lagarde, A. Balocchi, M. Vidal, T. Amand, X. Marie, B. Urbaszek, 2D Mater. 2 (2015) 045005.
[67] S. Tongay, J. Zhou, C. Ataca, K. Lo, T.S. Matthews, J. Li, J.C. Grossman, J. Wu, Nano Lett. 12 (2012) 5576-5580.
[68] Y. Lee, S.B. Cho, Y.-C. Chung, ACS Appl. Mater. Interfaces. 6 (2014) 14724-14728.
[69] I.G. Lezama, A. Arora, A. Ubaldini, C. Barreteau, E. Giannini, M. Potemski, A.F. Morpurgo, Nano Lett. 15 (2015) 2336-2342.
[70] Y. Shi, B. Guo, S.A. Corr, Q. Shi, Y.-S. Hu, K.R. Heier, L. Chen, R. Seshadri, G.D. Stucky, Nano Lett. 9 (2009) 4215-4220.
[71] J. Ni, Y. Zhao, L. Li, L. Mai, Nano Energy. 11 (2015) 129-135.
[72] B. Hu, L. Mai, W. Chen, F. Yang, ACS Nano. 3 (2009) 478-482.
[73] C. Ataca, H. Şahin, S. Ciraci, J. Phys. Chem. C. 116 (2012) 8983-8999.
[74] Z. Xiang, Q. Zhang, Z. Zhang, X. Xu, Q. Wang, Ceram. Int. 41 (2015) 977-981.
[75] P. Qin, G. Fang, W. Ke, F. Cheng, Q. Zheng, J. Wan, H. Lei, X. Zhao, J. Mater. Chem. A. 2 (2014) 2742-2756.
[76] A. Angelica, K.C. Santosh, P. Xin, L. Ning, M. Stephen, Q. Xiaoye, D. Francis de, A. Rafik, K. Jiyoung, J.K. Moon, C. Kyeongjae, M.W. Robert, 2D Mater. 2 (2015) 014004.
[77] H. Wang, D. Kong, P. Johanes, J.J. Cha, G. Zheng, K. Yan, N. Liu, Y. Cui, Nano Lett. 13 (2013) 3426-3433.
[78] A. Conan, A. Bonnet, A. Amrouche, M. Spiesser, J. Phys. 45 (1984) 459-465.
[79] A. Roy, H.C.P. Movva, B. Satpati, K. Kim, R. Dey, A. Rai, T. Pramanik, S. Guchhait, E. Tutuc, S.K. Banerjee, ACS Appl. Mater. Interfaces. 8 (2016) 7396-7402.
[80] C.A. Wolden, R.M. Morrish, Google Patents, 2015.
[81] A. Chen, C. Li, R. Tang, L. Yin, Y. Qi, Phys. Chem. Chem. Phys. 15 (2013) 13601-13610.
[82] E. Miliordos, S.S. Xantheas, Phys. Chem. Chem. Phys. 16 (2014) 6886-6892.
[83] E. Miliordos, S.S. Xantheas, Theor. Chem. Acc. 133 (2014) 1-12.
[84] O. Ghodbane, J.-L. Pascal, F. Favier, ACS Appl. Mater. Interfaces. 1 (2009) 1130-1139.